# Self-Ordering of Colloidal Particles in Shallow Nanoscale Surface Corrugations

Anant Mathur,† Ari-David Brown,† and Jonah Erlebacher*,†,‡

*Department of Materials Science and Engineering and Department of Chemical and Biomolecular Engineering, Johns Hopkins University, Baltimore, Maryland 21218*

*Received July 27, 2005. In Final Form: November 1, 2005*

The influence of nanoscale out-of-plane roughness on the ordering of submicron spheres during evaporative deposition from colloidal suspension was examined using shallow corrugated substrates possessing optical wavelengths and nanoscale amplitude. Under conditions in which spheres were embedded in a liquid layer with thickness on the order of the sphere diameter, it was observed that the spheres overwhelmingly deposited in the valleys of the surface corrugations rather than on their peaks. This behavior persisted to surprisingly shallow corrugation amplitudes, sometimes 100 times smaller than the sphere diameter. An analysis of the capillary forces on the spheres explains this behavior and also yields a critical corrugation amplitude below which a substrate will appear "flat" to depositing spheres. The observation that substrate features significantly smaller than the sphere diameter can influence deposition morphology may lead to simple methods to create large domains of order in colloidal crystals.

## Introduction

Colloidal particles have a long history of use in various industrial applications such as coatings, inks, drugs, paints, and cosmetics, besides foods and drinks.[1] Current interest in this field has been spurred by advances in the ability to synthesize monodisperse colloidal particles of uniform shape, composition, and surface properties. Colloids are now being used in numerous additional roles: for fabricating photonic band-gap structures, as physical masks in nanosphere lithography,[2,3] in making elastomeric stamps for soft lithography,[4] and for approximating and visualizing molecular-scale processes in crystal growth such as nucleation and dynamics of defects.[5,6] A central theme in many of these applications is crystallization from colloidal suspension to form one-, two-, and three-dimensional (1D, 2D, and 3D) arrays of submicron spheres (colloidal crystals).[7] Commonly, monodisperse spherical particles ranging in diameter from 20 nm to ∼1 $\mu$m made from silica or polystyrene (PS) latex are used in these applications.

In this work, we are concerned with the formation of 1D and 2D PS colloidal crystals on substrates patterned with a subtle 1D topography. As a general description, the formation of colloidal crystals on a solid surface is the outcome of an interplay between (i) the attractive capillary forces acting on partially immersed particles,[8] (ii) the convective flows carrying fully immersed particles, and (iii) the electrostatic interactions between spheres. Of these, electrostatic interacations are by far the weakest. Even though PS spheres are often functionalized with a range of endgroups such as $-NH_2$, $-COOH$, $-SO_3H$, etc.,[7] Aizenberg et al.,[9] for instance, have shown that for typical surface charges on PS nanospheres the free energy of capillary interaction of partially immersed spheres[10] is orders of magnitude larger than the electrostatic free energy. Indeed, addition of electrolytes that stabilize surface charges makes no notable difference to particle ordering; hence repulsive Coulombic interactions are insignificant compared to capillary forces.

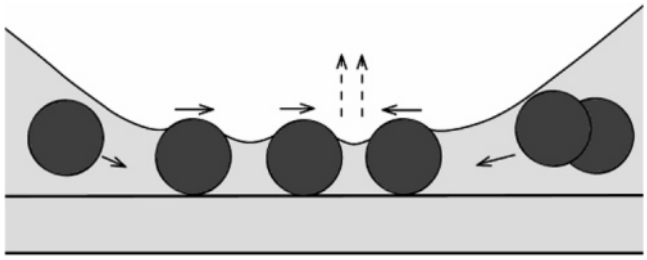

**Figure 1.** Cartoon illustrating the formation of a 2D nucleus inside the region for which the liquid layer thickness drops below the sphere diameter. Convective flow transports other particles to the nucleus and leads to growth of a 2D domain.

Denkov et al.[10] discussed capillary and convective forces acting on partially immersed spheres and how these lead to formation of domains of hexagonal close packed order. In their picture, attractive capillary forces between spheres lead to the formation of a nucleus which grows while being fed by a convective flow that transports other spheres toward it (as shown in Figure 1). For perfectly flat substrates, the in-plane orientation of these nuclei is random, and thus long-range order depends almost exclusively on controlling a low nucleation density. Strategies to this end include controlling evaporation kinetics and contact angles[11] and growing colloidal crystals on nearly *perfectly planar* surfaces such as mica and glass.[12,13] In contrast, our hypothesis is that if ordering can be imposed during nucleation itself, the nucleation density becomes unimportant—if all nuclei are oriented

* To whom correspondence should be addressed.
† Department of Materials Science and Engineering.
‡ Department of Chemical and Biomolecular Engineering.

(1) See, for example: (a) Everett, D. H. *Basic Principles of Colloid Science*; Royal Society of Chemistry: London, 1988. (b) Hunter, R. J. *Introduction to Modern Colloid Science*; Oxford University Press: Oxford, 1993.
(2) Hulteen, J. C.; Duyue, R. P. V. *J. Vac. Sci. Technol.* **1995**, *A13*, 1533.
(3) Burmeister, F.; Schafle, C.; Matthes, T.; Bohmisch, M.; Boneberg, J.; Leiderer, P. *Langmuir* **1997**, *13* (11), 2983−2987.
(4) Xia, Y. N.; Whitesides, G. M. *Langmuir* **1997**, *13*, 2059.
(5) Pertsinidis, A.; Ling, X. S. *Nature* **2001**, *413*, 147.
(6) Schall, P.; Cohen, I.; Weitz, D. A.; Spaepen, F. *Science* **2004**, *305*, 1944.
(7) Xia, Y. N.; Gates, B.; Yin, Y. D.; Lu, Y. *Adv. Mater.* **2000**, *12*, 693.
(8) Kralchevsky, P. A.; Paunov, V. N.; Ivanov, I. B.; Nagayama, K. *J. Colloid Interface Sci.* **1992**, *151*, 79.
(9) Aizenberg, J.; Braun, P. V.; Wiltzius, P. *Phys. Rev. Lett.* **2000**, *84*, 2997.
(10) Denkov, N. D.; Velev, O. D.; Kralchevsky, P. A.; Ivanov, I. B.; Yoshimura, H.; Nagayama, K. *Langmuir* **1992**, *8*, 3183.
(11) Conway, J.; Korns, H.; Fisch, M. R. *Langmuir* **1997**, *13*, 426.
(12) Dimitrov, A. S.; Dushkin, C. D.; Yoshimura, H.; Nagayama, K. *Langmuir* **1994**, *10*, 432.
(13) Adachi, E.; Dimitrov, A. S.; Nagayama, K. *Langmuir* **1995**, *11*, 1057.

10.1021/la0520379 CCC: $33.50 
Published on Web 12/17/2005

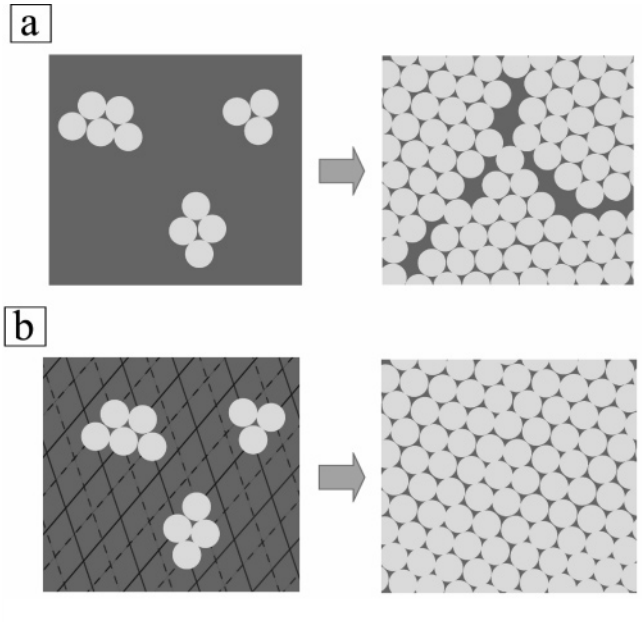


**Figure 2.** Cartoon illustrating the formation of large ordered domains on morphologically patterned substrates. (a) On featureless substrates, nucleation is random both spatially and in the relative rotation of each nuclei. (b) A two-dimensional substrate corrugation may template both the relative orientation of nuclei and the spacing between them so that they grow seamlessly into a large ordered domain.

the same and in fixed geometric registry, they will grow together and coalesce seamlessly to form large, coherent domains. This idea is illustrated as a cartoon in Figure 2.

The strategy we employ to control order in colloidal crystallization is to use substrates with very shallow corrugations, i.e., with amplitude significantly smaller than the sphere diameter. The smoothly varying corrugations provide a subtle driving force to orient colloidal crystal nuclei, but are shallow enough that long-range ordering can be established when each oriented nucleus grows and impinges on its neighbors. This approach differs from other "templating" methods in which sharp features such as channels or pits are created by lithography and colloidal particles "trapped" in these features exhibit good ordering; for example, such a strategy was used by Yin et al. to create controlled aggregates of PS spheres,[14] and more recently by Cheng et al. to create good order in block copolymer phase separation.[15] Fundamentally, most templating strategies attempt to create order by controlling the equilibrium thermodynamic state by creating a finite area over which crystallization can occur, whereas our strategy here is fundamentally kinetic and involves only control of nuclei orientation and can be conceptually extended to substrates of any area.

The substrates required for this study are uncommon. They consist of a smoothly varying, nearly sinusoidal corrugated array formed in the surface of silicon (with native oxide) via a spontaneous pattern-forming instability seen during simultaneous ion beam etching and substrate heating.[16] By changing the ion beam current relative to the substrate temperature, corrugation geometries with optical wavelengths (300−1000 nm), and nanoscale amplitudes (1−50 nm), may be easily and quickly fabricated. The phenomenon, so-called "sputter rippling", has been used to probe fundamental surface physics such as surface diffusion,[17] but has been particularly useful in this study because such small amplitude:wavelength aspect ratios are actually quite difficult to make lithographically. In contrast to other methods, sputter rippling can be used to routinely create areas of ∼5 $cm^2$ of sputter rippled substrate (the ion beam area) in a single sputter run, and the wavelength and amplitude are easily tuned simply by changing the sample temperature and/or the ion beam current.

Ideally, the substrate corrugations required for nuclei to be in registry both in period and in azimuthal orientation should be two-dimensional. However, here we are exploring the influence of only one-dimensional ripple corrugations. This morphology has the advantage of being easily producible with different nanoscale amplitudes, but provides only rotational registry between different nuclei, as we will show. Sputter rippled substrates, however, exhibit a wide variety of order, from very regular, highly aligned corrugations,[18] to more "wormy" features,[16] and even two-dimensional arrays of bumps;[19,20] further examination will probe the effect of these more highly ordered substrates.

In probing the effects of the substrate corrugation amplitude on the 1D and 2D ordering of colloidal spheres during evaporative deposition, we find primarily that the amplitude below which there is no influence of the substrate morphology is very small, on the order of 1 nm when the diameter of the spheres is greater than 100 nm. We argue that this is due to a *surface-mediated* capillary force that sensitively couples particle ordering to the surface morphology, and that this ordering force is significant except for the very smallest amplitudes. We determine a threshold roughness below which a surface is effectively "flat" to a depositing colloidal particle and show that this threshold conforms to a simple theoretical model consistent with our experimental observations.

## Experimental Section

**Sputter Rippled Substrates.** Corrugated Si(111) substrates are prepared by simultaneous ion beam etching (500−1000 eV, $Ar^+$) at 60° off normal and heating to between 600 and 700 °C in accordance with published recipes.[16−19] This technique is called sputter rippling, because after a period of etching, the surface becomes corrugated with a periodicity regular enough to be observed as a diffraction grating. The physics of such pattern formation are discussed elsewhere.[21] For the samples used here, sputtering was done in an ultra-high-vacuum chamber (base pressure $10^{-10}$ Torr) on 3 in. diameter wafers to produce rippled areas of ∼5 $cm^2$. Upon removal from the chamber a native oxide with thickness on the order of 10 nm quickly forms on the silicon wafers, which were then used as substrates without any further processing. The wavelength and amplitude (half of peak-to-valley) of these ripples are controlled by the ion energy and silicon temperature. In this experiment, we adjusted these experimental parameters to produce substrates with wavelength of approximately 600 nm. With this wavelength, amplitudes at the extremes of the approximate range of 2−30 nm were used; in this way, we produced what we term "large" (∼30 nm amplitude) and "small" (∼2 nm) ripples. Figure 3 shows micrographs of surfaces with large and small ripples.

**Colloidal Crystallization.** Colloidal suspensions of 100, 200, and 500 nm diameter polystyrene (PS) spheres [AlfaAesar, 2.5% v/v] in water were further diluted in clean water (Millipore Milli-Q, 18.2 MΩ, 2 ppb total organic content (TOC)) in dilutions of 1:100

(14) Yin, Y.; Lu, Y.; Gates, B.; Xia, Y. *J. Am. Chem. Soc.* **2001**, *123*, 8718.
(15) Cheng, J.; Ross, C. A.; Mayes, A. *Nat. Mater.* **2004**, *3*, 823.
(16) Erlebacher, J.; Aziz, M. J.; Chason, E.; et al. *Phys. Rev. Lett.* **1999**, *82*, 2330.
(17) Erlebacher, J.; Aziz, M. J.; Chason, E.; et al. *Phys. Rev. Lett.* **2000**, *84*, 5800.
(18) Brown, A. D.; Erlebacher, J. *Phys. Rev. B* **2005**, *72*, 075350.
(19) Brown, A. D.; Erlebacher, J.; et al. *Phys. Rev. Lett.* **2005**, *95*, 056101.
(20) Facsko, S.; Dekorsy, T.; Koerdt, C.; et al. *Science* **1999**, *285*, 1551.
(21) Makeev, M.; Cuerno, R.; Barabási, A. L. *Nucl. Instrum. Methods Phys. Res., Sect. B* **2002**, *197*, 185.

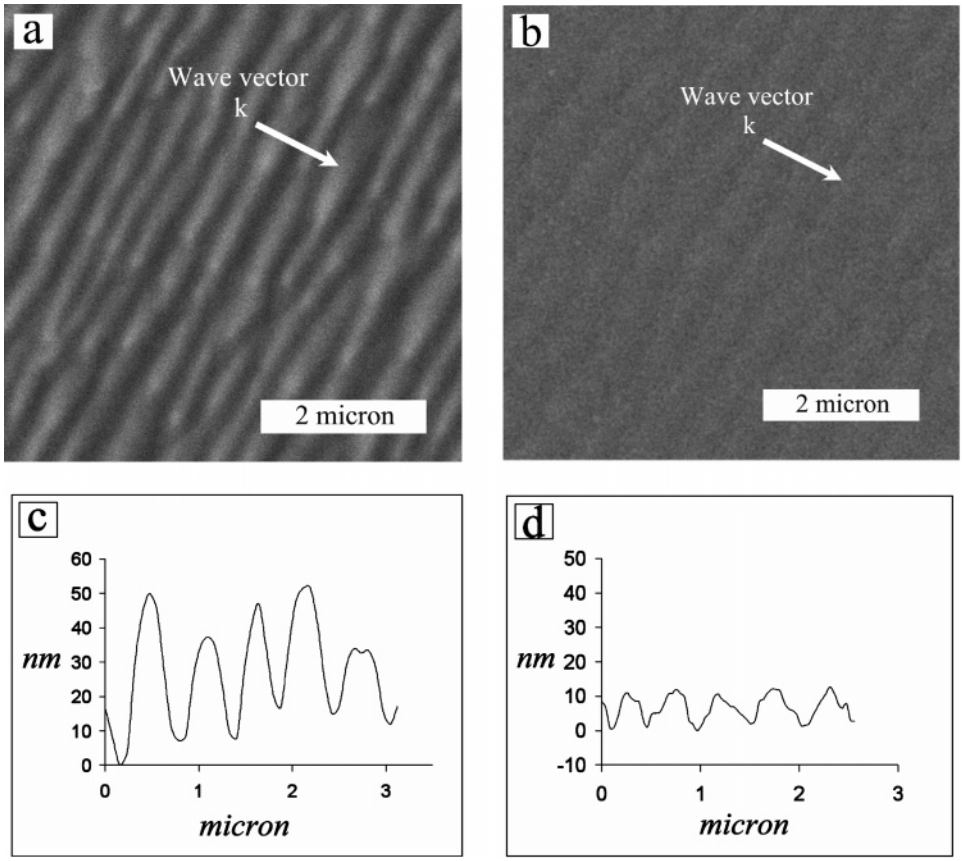


**Figure 3.** Typical sputter rippled substrate morphologies. (a) SEM of large amplitude ripples: the peaks appear bright while the valleys appear dark. (b) SEM of small amplitude ripples: the contrast between peaks and valleys is small. (c) AFM profile of large amplitude ripples: amplitude ~20 nm and wavelength ~700 nm. (d) AFM profile of small amplitude ripples: amplitude ~5 nm and wavelength ~500 nm. The wave vector *k* of the corrugation serves to orient the morphology.

and 1:1000 to get overall colloid concentrations of $2.5 \times 10^{-4}$ v/v and $2.5 \times 10^{-5}$ v/v, respectively. Prior to use, rippled substrates were cleaned by ultrasonication in clean water for 10 min, followed by a rinse under running clean water for 5 min in order to remove dust and particulates, and then air-dried in a desiccator. Droplets of colloidal suspension with 5 $\mu$L volume were placed on the substrate using a micropipet to form droplets of diameter roughly 2−3 mm, which were allowed to evaporate slowly under natural convection inside the desiccator. As the water evaporates, the spheres are deposited by adhering strongly to the substrate in regions where the suspension has sufficiently thinned. For in situ observation of the evaporating droplet, some samples were removed from the desiccator and mounted on an inverted stage optical microscope (Olympus PMG-3). In these samples, heat from the microscope lamp caused a noticeable enhancement in the kinetics of evaporation; however, the colloid particle ordering was found to evolve exactly as it does on other (nonilluminated) samples.

Once evaporation of a droplet was complete, samples were mounted in a scanning electron microscope (SEM, JEOL6700F) for observation. Since the PS spheres are nonconductive, a low accelerating voltage of 5 kV was used for imaging. To best capture morphological features of the substrate, the SEM was operated in the lower secondary electron image (LEI) mode, with the sample stage tilted 18° toward the detector. Samples were also examined using an atomic force microscope (AFM, Digital Instruments, Nanoscope III) operated in tapping mode.

## Results and Discussion

**Experimental Results.** In situ observation of evaporating droplets showed typical behavior also seen on flat substrates.[22−24] Initially, we observed the formation of a multilayered "ridge" of spheres at the perimeter, a "coffee-ring" effect due to strong convective flow and increasing sphere concentration toward the contact line. This accretion ridge in turn pins the contact line. As more water evaporates, we note a thinning of the drop (evident from the appearance of "Newton's rings") near the perimeter, followed by a depinning event in which the contact line rushes inward from the perimeter, allowing the droplet to reduce its surface area. At some point the contact line again becomes static for an interval of time during which edge deposits build up once again, causing further pinning. This is again followed by a depinning event, after which the contact line again rushes radially inward, and so on. At the end, we get approximately concentric circles of large, quasi-close-packed, 3D deposits of spheres.[25]

Between the concentric rings, i.e., the pinning positions, are "slip zones" that evolve as follows. First, during depinning events the "bulk" contact line quickly moves through the slip zone. However, second, we observe that the area of the slip zone does not become instantly dry; rather, a thin layer of water remains with a blue appearance indicating that its thickness is on the order of the size of the colloidal spheres that happened to be left in the slip zone. The areal density of these spheres is always less than 1 monolayer (ML). Third, the initial configuration of these spheres is random in-plane until, fourth, the thin water layer evaporates, at which point we see that the spheres in the slip zone are now ordered relative to the substrate corrugations.

The ordering of spheres during the final evaporation of the water layer in the slip zone is of central interest to us because,

(22) Deegan, R. D.; Bakajin, O.; Dupont, T. F.; Huber, G.; Nagel, S. R.; Witten, T. A. *Nature* **1997**, *389*, 827.
(23) Shmuylovich, L.; Shen, A. Q.; Stone, H. A. *Langmuir* **2002**, *18*, 3441.
(24) Fan, F. Q.; Stebe, K. J. *Langmuir* **2004**, *20*, 3062.
(25) Abkarian, M.; Nunes, J.; Stone, H. A. *J. Am. Chem. Soc.* **2004**, *126*, 5978.

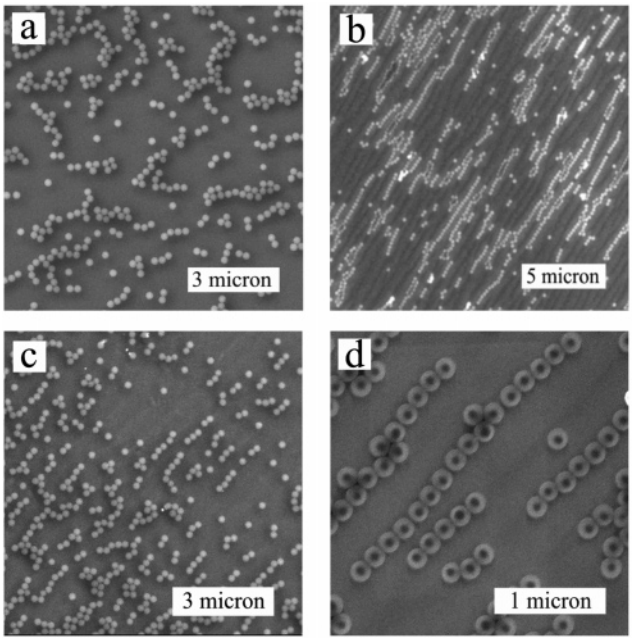


**Figure 4.** SEM micrographs. (a) 200 nm PS spheres deposited on a *flat* Si surface tend to form 2D clusters with no particular orientation. (b) 200 nm spheres deposited on large amplitude ripples form 1D "pearl chains" in ripple valleys. (c) Deposition on small amplitude ripples also shows pearl chain deposition of spheres. (d) Higher magnification of a pearl chain shows that the spheres are in contact with each other (the dark centers are an artifact, and due to SEM charging effects).

unlike the denser (>1 ML) areas such as the accretion regions, effects of the substrate's morphology are evident here. In all our experiments we find that spheres in the low-density areas have an overwhelming tendency to deposit in the valleys of the rippled surface rather than the peaks. Serving as a control, we observe a random arrangement of spheres found after evaporation on a flat surface (Figure 4a). In contrast, on the rippled surface we see formation of "pearl chains", i.e., 1D crystals inhabiting ripple valleys. Examples are shown in Figure 4b−d. The spheres in these chains abut each other. Chains as long as 50 spheres can be seen on some samples; in general, chains are between 2 and 20 spheres long. The lengths of the chains appear to be limited by the length of the underlying valley. Closer to edges of the slip zones where sphere density is higher, although still less than 1 ML, we see elongated 2D arrays inhabiting the valleys rather than the 1D chains seen in the central portions of the slip zones. We find that pearl-chains of 200 nm diameter spheres are formed in ripples with amplitudes as small as 3 nm! The pearl chains are clearly aligned with the ripples and have the same orientation over the entire area of the sample. Because the circular perimeter of the evaporating droplet varies radially relative to the fixed, static orientation of the substrate corrugation, these pearl chains are *not* frozen-in residues of convection-driven radial motion of the spheres.

In samples with the lower colloid concentration ($2.5 \times 10^{-5}$ v/v), regions of very low density deposits in the slip zones are found. Spheres depositing in these zones can be considered isolated and free of particle−particle interactions. As shown in Figure 5, *each* isolated sphere is also found to settle in a valley, and this behavior is repeated for ripples as small as 3 nm in amplitude. This indicates that the ordering in the low sphere density limit is influenced by the substrate alone, rather than a correlated ordering phenomenon involving sphere−sphere−substrate interactions.

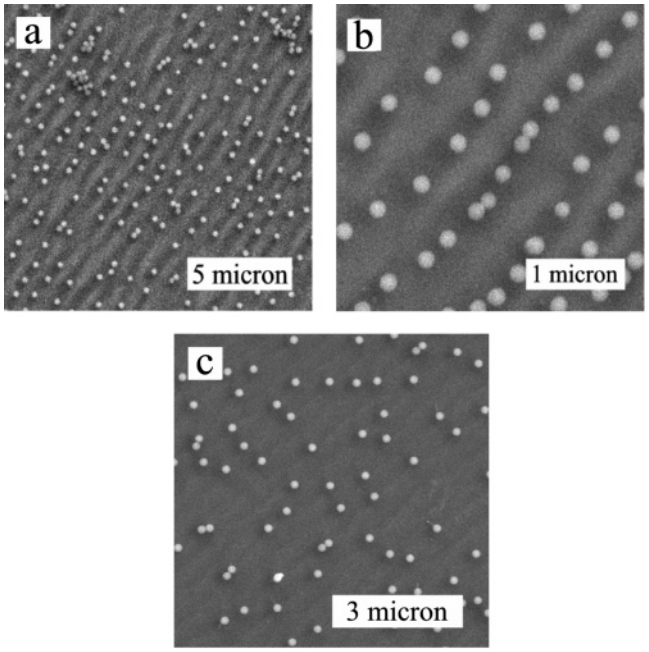


**Figure 5.** SEM micrographs of isolated spheres in (a, b) *large* amplitude ripples and (c) *small* amplitude ripples. The spheres clearly inhabit ripple valleys.

We find that pearl-chain ordering in the slip zones is quite robust and easily reproduced in a variety of experimental setups. Experiments were performed where the rippled surface was immersed vertically (or at angle) in an evaporating bath of colloidal suspension, where the evaporation of a droplet on substrate was carried out with the sample upside down, and where the droplet evaporation was accelerated by heating on a hot plate at 85 °C. In each case the ordering behavior was found to be identical.

Under extreme driving forces, sphere ordering can be disrupted. The PS spheres we used had a slight anionic surface charge. We performed deposition under an applied electric field by applying a +3 V dc potential to the Si substrate relative to another Si electrode, both partially immersed in a bath of colloidal suspension. A visible increase in the sphere concentration was observed at the contact line, and thick bands of 3D deposits separated by thinner slip-zone regions were obtained. In areas where coverage was 1 ML, the spheres were close-packed with an orientation that did not depend on the corrugated substrate morphology, i.e., as if the deposition had been carried out on a flat surface. When the applied voltage is reversed, sphere density at the contact line is dramatically reduced, and spheres are more or less absent from the drying Si surface. Finally, absence of ordering is also seen if evaporation of a droplet on substrate is carried out at temperatures close to 100 °C, an effect likely due to the turbulent motion of water and vapor during evaporation at this temperature.

**Analysis of Capillary Forces on Spheres in Shallow Corrugations.** The ordering motion of spheres from peaks to valleys is interesting because gravity, the obvious cause of such a phenomenon at the macroscale, does not play a role here; gravitational effects are insignificant compared to capillary interactions, the dominant force at this scale. Indeed, sphere ordering is reproduced regardless of sample orientation in the gravitational field (including upside down). Also, unlike traditional 1D/2D self-assembly where colloid particles are "trapped" in features *larger* than the particle size, here we have ordering of spheres in features that are *significantly smaller* (∼one hundredth the size) than the particles themselves. Because in situ

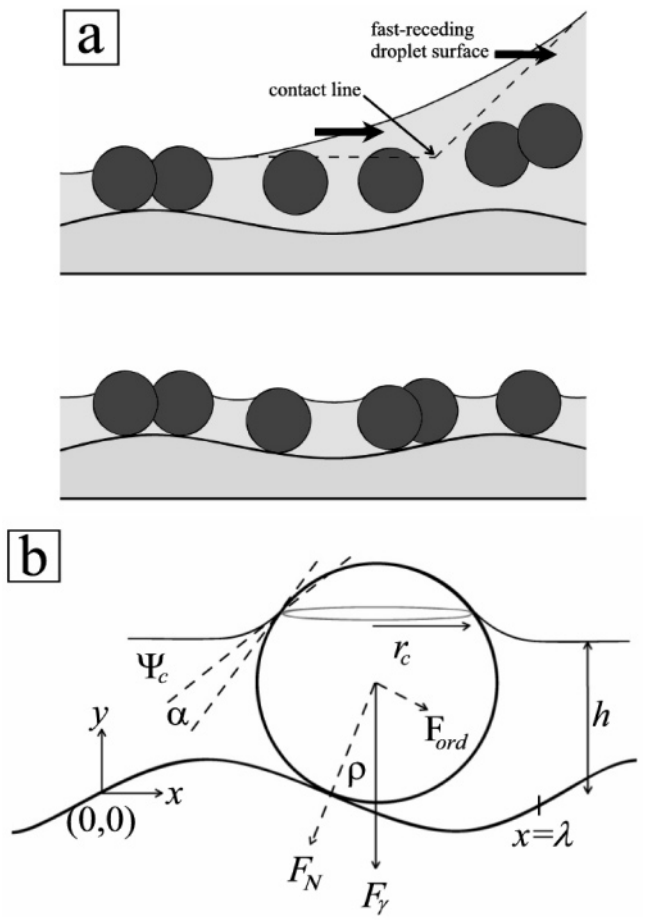


**Figure 6.** Cartoon illustrating (a) randomly distributed spheres as initially deposited on a ripple profile (not to scale) and partially immersed in an evaporating water film. (b) Geometry of a sphere sitting at an arbitrary position on a ripple, and the forces acting on it. See text for explanation of variable quantities.

observation shows that evaporation of the water film occurs through nucleation and growth of dry zones, we can eliminate preferential spinodal dewetting[26] of the water film along the ripple peaks as a possible cause of this ordering behavior.

In the slip zone, the moving contact line exerts a lateral force on the spheres radially inward toward the center. Thus, if the contact line motion were quasi-static, all spheres would be continually pulled into the bulk. However, the contact line moves inward quite rapidly after a depinning event, while at the same time there is a net outward flux of spheres due to convective flow in the droplet. In conjunction with frictional forces acting on partially exposed spheres, this impedes inward sphere motion. When the bulk contact line has moved to its next quasi-equilibrium position, it has left behind partially exposed, randomly distributed spheres embedded in a fast evaporating thin film of water that is less than one sphere diameter in thickness (Figure 6a). The appearance of this thin film is observable under the optical microscope. For instance, using the 200 nm diameter spheres, the thin water film appears a uniform blue under the unpolarized light of an optical microscope. It is this thin film that exerts the surface-mediated lateral capillary force on the spheres and leads to ordering.

Within a film of water thinner than the sphere diameter, partially exposed spheres are mobile in the surface plane and subject to forces due to the surface tension of water, as shown in Figure 6b. We now show how surface tension preferentially transports spheres situated at any point other than a valley toward the nearest valley position. For each sphere, the length of the contact line is the circumference of the circle of radius $r_c = [H(2R - H)]^{1/2}$, where $R$ is the radius of the sphere and $H$ is the height of the water film. Surface tension $\gamma$ acts on this line at an angle $\alpha$ (the contact angle) from the tangent to the sphere at that point. The vertical component of surface tension acting on the sphere, i.e., the downward pinning force, is given by $F_\gamma = \gamma(2\pi r_c) \sin \Psi_c$, where $\Psi_c = \arcsin(r_c/R) - \alpha$ is the mean slope angle of the meniscus at the contact line. The component of $F_\gamma$ normal to the local surface is $F_N = F_\gamma \cos \rho$, where $\rho$ is the angle between the tangent and the horizontal axis (i.e., $x$ axis) at the local point of contact between the sphere and the substrate; $F_N$ is balanced by a reaction from the substrate. However, the component tangent to the local surface profile is unbalanced and provides the motive force for sphere movement toward the valley. We call this the "ordering force" $F_{ord}$, given as $F_{ord} = F_\gamma \sin \rho$. Geometrically, $\rho = \arctan(d\xi/dx)$, where $\xi = \eta \sin(kx)$ describes the surface profile of the substrate. We approximate the surface profile as perfectly sinusoidal with wave vector $k = 2\pi/\lambda$, where $\lambda$ is the wavelength of the sinusoid. Simplifying, we have $\rho = \arctan[\eta k \cos(kx)]$. Therefore

$$F_{ord} = \gamma(2\pi r_c) \sin \Psi_c \sin\{\arctan[\eta k \cos(kx)]\} \qquad (1)$$

From geometry, we note that

$$\sin\{\arctan[\eta k \cos(kx)]\} = \frac{\eta k \cos(kx)}{\sqrt{1 + (\eta k)^2(\cos(k\cdot x))^2}}$$

so that eq 1 can also be written as

$$F_{ord} = \gamma(2\pi r_c) \sin \Psi_c \frac{\eta k \cos(kx)}{\sqrt{1 + (\eta k)^2(\cos(kx))^2}}$$

For an estimate of $F_{ord}$, consider a 200 nm diameter PS sphere located at $x = 0$ on a substrate with $\lambda = 600$ nm and amplitude $\eta = 30$ nm. Using the surface tension of water, $\gamma = 72$ dyn/cm, and contact angle $\alpha = 30°$,[10] we find that at $H = 100$ nm (i.e., half submersion of the sphere), $F_{ord} = 1.174 \times 10^{-8}$ N. Because the mass of a sphere $m = 4.4 \times 10^{-18}$ kg, the ordering force is very large compared to the gravitational forces, as expected.

To calculate forces inhibiting sphere motion, we may consider the sphere to be in contact with the substrate (i.e., assume no water layer exists between the sphere and the substrate) and estimate the static friction on the sphere. In this model, the frictional force on the sphere is given as $F_f = \mu F_N = \mu\gamma(2\pi r_c) \sin \Psi_c \cos \rho$, where $\mu$ is the coefficient of friction between the polystyrene sphere and the substrate. We can therefore write the ratio

$$\frac{F_f}{F_{ord}} = \mu \cot \rho$$

A reasonable estimate for $\mu$ is ~0.2,[27] which means that for small $\rho$ (as is typically the case in these experiments) $F_f > F_{ord}$, which predicts that the sphere should not move at all due to friction. The evidence, experimentally, is to the contrary: spheres *always* move to valley positions, even for vanishing $\rho$. Therefore, static friction must be absent here, implying the presence of a thin water layer *between* the sphere and the substrate. In this case, a velocity-dependent viscous drag, rather than sphere−

(26) Wyart, F. B.; Daillant, J. *Can. J. Phys.* **1990**, *68*, 1084.

(27) Michel, D.; Kopp-Marsaudon, S.; Aime, J. P. *Tribol. Lett.* **1998**, *4*, 75.

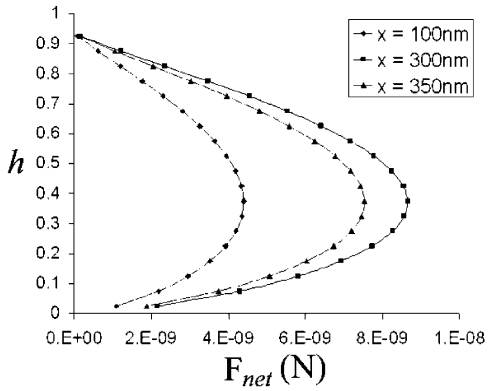


**Figure 7.** Calculated net force acting on an isolated sphere vs thickness of water film height for various values of corrugation amplitude $\eta$. A large ordering force acts at all positions (values of $x$) along the surface for all thicknesses of water film height, driving the sphere toward the valley.

substrate friction, is the force inhibiting motion and is given by the Stokes drag law. A precise calculation of the drag coefficient is complicated due to the presence of adjacent boundaries, and is not attempted here. Also, the dynamic nature of the drag is incompatible with the statics approach adopted here. However, based on experimental evidence, it is easy to conclude that the drag force $F_d$ on the sphere is very small compared to $F_{ord}$, so that $F_d = \epsilon F_{ord}$, where $\epsilon \ll 1$. Therefore, we can approximate the *net* force acting on a single sphere on large magnitude ripples as $F_{net} = F_{ord} - F_d \approx F_{ord}$.

Clearly, the magnitude of $F_{ord}$ depends on the position of the sphere along the surface. There are two positions of minimal (zero) force: the peak ($x = \lambda/4$ in our coordinate system) and the valley ($x = 3\lambda/4$). However, spheres situated at the peak are in unstable equilibrium and any perturbation subjects them to a positive $F_{ord}$ toward the valleys. The valley is the only position of stable equilibrium. Figure 7 shows a plot of $F_{net}$ ($R = 100$ nm, $\eta = 20$ nm, $\lambda = 600$ nm) as a function of the water film height $h$ (normalized with respect to sphere diameter, i.e., $h = H/2R$) at different locations on the surface. We observe that a large, continuous ordering force acts at all positions along the surface and for all thicknesses of the water film, driving spheres into the valleys.

In our discussion here, we assume that the time of travel of a sphere from an arbitrary position along the surface profile to the bottom of the nearest valley is less than the time of evaporation of a water film of height equal to the sphere diameter. While we have not studied the kinetics of film evaporation and sphere transport in much detail, we estimate from our observations that the time of evaporation of a 200 nm water film in ambient conditions is on the order of 0.1 s. A rough estimate for the time of travel of an arbitrary sphere to the nearest valley can be written as $t = \lambda/v$, where $\lambda$ is the ripple wavelength as before and $v$ is the sphere velocity. An approximation for $v$ can be obtained by using Stokes law $F_d = 6\pi R\tau v$, where we assume $\epsilon = 0.1$, so that $F_d = 0.1F_{ord}$. Here $R$ is the sphere radius and $\tau$ the liquid viscosity. Using $\tau = 8.9 \times 10^{-4}$ N m/s$^2$ for water, and values for other parameters as before, we find $t \sim 10^{-6}$ s. This estimate of $t$ gives an idea of the time scale of sphere travel; even if $t$ is a few orders of magnitude larger, it would still be much smaller than the film evaporation time.

The analysis so far explains the ordering of *isolated* spheres where the surface-mediated capillary force is the only active force (besides friction, of course), and is thus primarily relevant for our low-density deposits. We now consider sphere−sphere interactions relevant for higher density deposits. We explain how ordering occurs in high-density regions much as it does in the low-density regions, and we discuss the role of strong sphere−sphere capillary attraction in the process. Finally, we discuss ordering in small amplitude ripples.

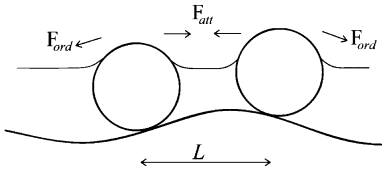


**Figure 8.** Cartoon illustrating two spheres separated by a ripple peak, with the sphere spacing $L$ smaller than the ripple wavelength $\lambda$. The net unbalanced force on each sphere is the sum of the ordering force $F_{ord}$ and the tangential component of the sphere−sphere attractive force $F_{att}$. For $L$ less than the characteristic length scale $l_c$ of the system, $F_{att} > F_{ord}$ and the spheres agglomerate to form a cluster.

Capillary interactions *between* any two partially immersed spheres may be taken into account as an "attractive capillary force"; this force was shown to be[8,10]

$$F_{att} \approx 2\pi\gamma r_c^2(\sin^2\Psi_c)(1/L) \qquad (2)$$

and is valid for $L \gg r_c$, where $L$ is the distance between the spheres. At short intersphere separations, $F_{att}$ acting on a sphere is large in magnitude compared to $F_{ord}$ arising from the typical ripple morphology. Since $F_{att}$ scales inversely with $L$ while $F_{ord}$ is independent of $L$ (it depends on position of sphere, not distance), we anticipate that a given system (i.e., fixed $\gamma$, $\alpha$, $\eta$, $x$, $R$) has a characteristic length $l_c$ below which $F_{att}$ dominates in magnitude over $F_{ord}$, and at distances greater than which $F_{att}$ becomes insignificant compared to $F_{ord}$. With a view to get an idea of the scale of $l_c$, we construct a scenario where $F_{ord}$ and $F_{att}$ are in competition, for example, when two spheres separated by distance $L$ are situated on opposite sides of a single peak (see Figure 8). Here, the ordering force tries to push them apart toward their respective valleys, whereas the attractive capillary force between them tries to pull them together to form a "dimer". We can write the net force acting on a particular sphere as a vector sum of the individual forces on it; we associate a negative sign with $F_{att}$ and a positive sign with $F_{ord}$, so that $F_{net} = (F_{ord} - F_{att}) \pm F_d$. The drag force $F_d$ always resists motion and its sign is opposite to the sign of the term in parentheses. Substituting expressions developed earlier, we find

$$F_{net} = \gamma 2\pi r_c \sin\Psi_c[(\sin\{\arctan[\eta k\cos(kx_0)]\} - r_c\sin\Psi_c/(x' - x_0))] \pm F_d \qquad (3)$$

where $x_0$ is the coordinate of the subject sphere and $x'$ is the coordinate of the sphere a distance $L$ away. We note that, for small $x' - x_0$, $F_{net}$ will be negative, and as $x' - x_0$ increases so does $F_{net}$. At the value of $x' - x_0$ corresponding to $l_c$, $F_{net}$ will become zero; therefore, to compute the value of $l_c = x' - x_0$, we set $F_{net} = 0$ and work backward. For simplicity, we do this computation only for $H = R$ (i.e., when each of the forces is near its maximum value), which corresponds to $r_c = R$, and only for the value of $x_0$ corresponding to the maximum $F_{ord}$, which is $x_0 = 0$ in our coordinate system. Also, we neglect $F_d$ because it is much smaller than $F_{ord}$ and $F_{att}$. Therefore, for $x_0 = 0$ we have

$$0 = \sin[\arctan(\eta k)] - (R\sin\Psi_c)/l_c$$

Using values of parameters as before—$\lambda = 600$ nm, $\eta = 30$ nm, $\alpha = 30°$—we find $l_c \approx 300$ nm. Roughly speaking then, this system has a characteristic length $l_c$ of order $\sim\lambda$ which provides

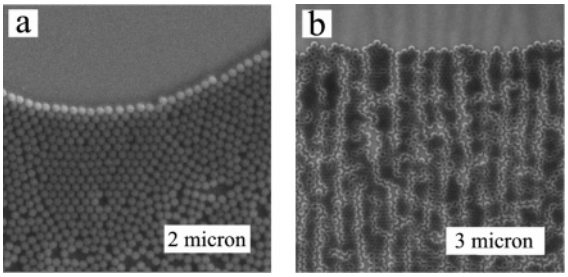


**Figure 9.** SEM micrographs. (a) Region of 1 ML coverage on *flat* Si: close-packed 2D domains within the region have no particular orientation. (b) Region of 1 ML coverage on rippled Si with amplitude ~15 nm: close-packed domains are aligned with the ripples.

a quantitative measure of "high" or "low" sphere density: if the mean intersphere spacing $L$ is less than $l_c = \lambda$, the sphere density is high; otherwise the system is low density and the spheres are more or less free of attractive capillary interactions.

Having defined a high-density region as where attractive capillary forces exceed the ordering force in magnitude, we discuss the ordering process in these regions. At first look it may appear that, because of the dominance of the attractive capillary force, spheres in these regions should agglomerate to form clusters of various sizes, without much heed to the underlying substrate morphology. Since the initial distribution is random, the probability of cluster formation at peaks and valleys would be equal; consequently, one expects a fairly random distribution of sphere clusters in the high-density regions upon evaporation. It is interesting, then, that our observations are to the contrary: we find that sphere ordering in high-density regions occurs with the same fidelity as the low-density areas, without exception. In fact, we see ordering in regions with density all the way to about 1 ML. Figure 9a is a micrograph of a region of 1 ML coverage on flat Si that shows several randomly oriented close-packed domains, while Figure 9b shows a ~1 ML coverage region on a rippled surface, where the close-packed domains are found to be aligned with the ripples. The edges of the 1 ML regions are also qualitatively different in the two cases.

A closer look at the ordering process in the high-density regions reveals that the attractive and ordering capillary forces are not perpetually in competition, as may appear to be the case initially. In fact, the attractive capillary force counters the ordering force only in the initial stages of evaporation, during which it pulls the spheres together; after that it merely holds them together while they collectively move under the position-dependent ordering force. To understand how ordering occurs in the high-density regions, consider a pair of spheres initially separated by a peak, as in Figure 10. During early evaporation, the large attractive force between the spheres overcomes the ordering and drag forces on each, and the spheres get pulled together to form a "dimer". However, this dimer is now subject to a similar ordering force as the spheres individually. Of course, the magnitude of $F_{ord}$ acting on the dimer is not simply a sum of the $F_{ord}$ on the individual spheres, owing to the asymmetry of the meniscus around the dimer. However, it is clear that a net ordering force does operate on it, pushing it toward the valley. The dynamics are now described by the net force acting on the new mobile species, the dimer: $F_{net} = F_{ord} - F_d$, which is qualitatively the same equation as for an isolated sphere, with the difference that terms on the right now represent *total* ordering and drag forces on the dimer rather than an individual sphere. As in the case of isolated spheres on large ripples, $F_{ord}$ for the dimer is typically much larger than $F_d$, and thus it is transported to the valley. Once it reaches the valley, the dimer may straddle across it, or in fact, more commonly, it may *rotate* to align with the valley (see Figure 11a). The rotation is expected to occur in the large majority of cases where the dimer axis is not orthogonal to the valley itself, so that $F_{ord}$ leads to a net moment of force, or torque, which aligns the dimer with the valley.

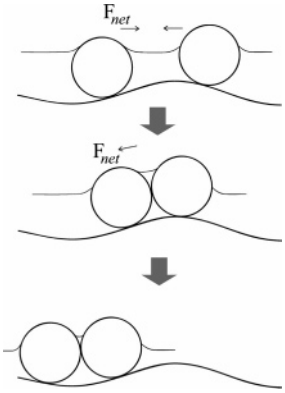


**Figure 10.** Cartoon illustrating formation of a cluster near a peak and its migration to the valley. Initially, the attractive capillary force between the spheres dominates, leading to the formation of a cluster, in this case a dimer. Once the cluster is formed, the attractive capillary force merely holds the spheres together and plays no role in the motion of the cluster which moves according to the total ordering force operating on it. The cluster finally comes to rest in the valley.

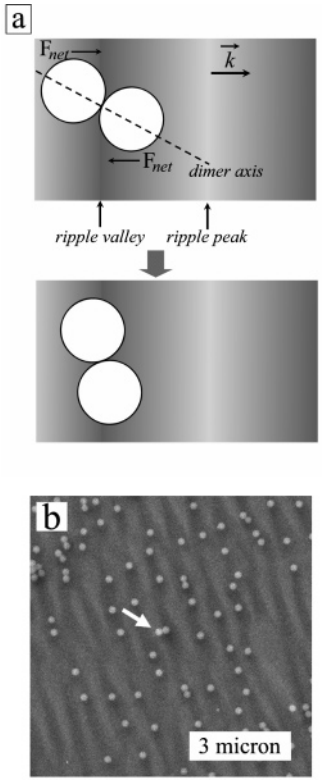


**Figure 11.** Cartoon illustrating alignment of a dimer with a valley, and an SEM micrograph of an immobile dimer at a ripple peak. (a) Plan view of a dimer in a ripple valley. Most dimers make angles not exactly equal to 90° with respect to the to valley, so the ordering force on each sphere provides a torque about the center and aligns the dimer with the valley. (b) SEM of a rare "peak dimer". Once this cluster is formed under the effect of the attractive capillary force, it remains immobile because it straddles the peak symmetrically: the spheres sit on opposite sides of the peak.

The mobile species is not limited to dimers—it may also include trimers and clusters of larger size. For obvious reasons, the largest mobile cluster is expected to be of dimension ~$\lambda$; clusters larger than that experience no net ordering force and are more or less immobile. The only scenario where a *small cluster* may be

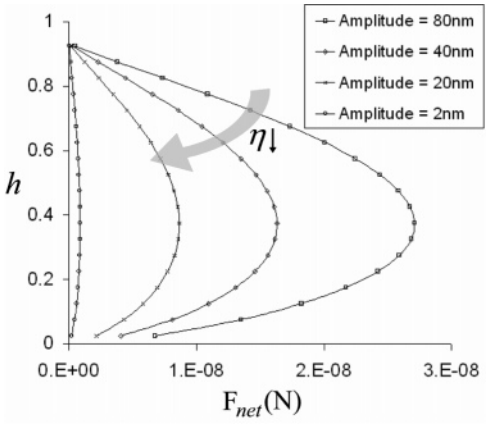


**Figure 12.** Calculated plot showing the ordering force $F_{net}$ vs water film height $h$ (normalized with respect to sphere diameter), for selected values of ripple amplitude $\eta$. It is seen that $F_{net}$ decreases almost linearly with $\eta$.

immobile (and therefore refuse to order in a valley) is when it straddles a peak in exact symmetry, so that the ordering force on each half is equal and opposite to that on the other half. In the case of a dimer, this happens when each of the two touching spheres sits exactly on opposite sides of the peak, which is an infrequent occurrence. Figure 11b shows one such "peak dimer". The likelihood of larger clusters becoming immobile in this fashion decreases rapidly with cluster size, and we did not observe large peak clusters in our experiments.

The formation of 1D pearl chains in the valleys is attributable to the unimpeded attractive capillary force that operates between a linear array of spheres already assembled in the valley by the ordering force. Consider a number of such spheres aligned along the valley, but not necessarily abutting each other. Since they no longer experience any ordering force, the attractive capillary interaction operates unimpeded (except for drag), so that the spheres pull together to form 1D "pearl chains".

Finally, we consider the sensitivity of sphere ordering to ripple amplitude. As noted before, we observe sphere ordering in ripples with amplitude as small as $\eta \sim 3$ nm. This behavior can be understood in the following way. From eq 1, we know that $F_{ord}$ scales with $\eta$. Figure 12 shows a plot of $F_{ord}$ (on an isolated sphere at $x = 0$) for decreasing $\eta$; the dependence is almost linear. As a result, when $\eta$ reduces from 20 to 2 nm, $F_{ord}$ reduces by about an order of magnitude as well. In a high-density region, the attractive interaction of the spheres remains qualitatively unchanged (since $F_{att}$ is independent of $\eta$), but the characteristic length scale $l_c$ of the system increases. This leads to formation of larger clusters which are immobile under the diminished ordering force. In a low-density region, on the other hand, cluster formation does not occur and the spheres are transported to the valleys as before, and sphere ordering continues to take place.

## Conclusions

We have demonstrated that large colloidal particles are remarkably sensitive to vanishingly small perturbations of a solid's surface, to the extent that a sphere can "detect" a nonplanarity almost 2 orders of magnitude smaller in amplitude than its diameter, spread out over a wavelength as large as 2−3 times the diameter. We have shown that the sensitivity is driven by the surface tension of the solvent in the colloid, in our case water, and its upper limit is most likely determined by viscous forces acting on the particles. The interparticle attractive capillary force which decays inversely with distance plays a qualitatively unimportant role in the ordering process. This type of surface-tension driven ordering behavior is seen for roughness amplitudes down to a few nanometers, and for concentrations all the way to almost 1 ML.

Finally, we address the issue of how the results presented here may aid the creation of long-range order in colloidal crystallization. To create truly large domains of order taking advantage of ordered nuclei on shallow nanoscale corrugated surfaces, we see two options: (i) create large areas over which the solution is on the order of the sphere diameter so that deposition everywhere is initially influenced by the substrate, or (ii) create regions of ordered nuclei during an initial evaporation using a corrugated substrate, and then use successive evaporations to grow these nuclei together so that they coalesce into larger ordered domains. Of these options, the latter strikes us as more viable. We recognize that somewhat more ordered substrates are still required so that the pearl chains are straighter, but the observations reported here still point to a new kinetic path to order in colloidal crystallization.

**Acknowledgment.** Support by the U.S. Department of Energy under Award No. DE-FG02-01ER45942 is gratefully acknowledged.

LA0520379